

STUDIES OF PERFORMANCE AND FIELD REPRODUCIBILITY OF A PRECISION 40KG SUPERCONDUCTING
DIPOLE MAGNET

J. Allinger, G. Danby, B. DeVito, S. Hsieh, J. Jackson, A. Prodell
Brookhaven Nat'l. Laboratory, Upton, L.I., N.Y.

Abstract

An 8° bending magnet system for 30 GeV primary protons from the Brookhaven AGS is to be installed in the summer of 1973. This bend requires operating two magnet modules, each 6-ft. long, at an excitation up to 37kG. The cold bore I.D. is 3.375-in. A 20-in. long full-scale cross section model has been extensively tested. Multipole field components due to the magnet circuit, produce field error $\sim 1 \times 10^{-4}$ parts below 20kG out to the measurement radius at 82% of the radius to the superconductor. The "good field" ($\sim 1 \times 10^{-4}$ parts) shrinks to a radius $\sim 50\%$ of the radius to the superconductor by 40kG. Diamagnetic effects in the superconductor are completely negligible by 5kG, with the exception of the (r^2 , 5θ) multipole. This contributes 6.5×10^{-3} parts to the field at 82% of radius. End effects are sufficiently small that for 6-ft. long magnets little or no modifications of end contours are required for even very exacting applications.

The magnet has operated to 45kG with no evidence of significant training. The magnet has been thermally cycled several times, and the field aberrations allowed by magnet design symmetries reproduce exactly from the first to last measurement runs. At 19.1kG, all allowed multipoles, i.e., $5\theta, 7\theta, 9\theta, 11\theta$, with 3θ tuned to zero agree to 1×10^{-4} parts error over the duration of experimental measurements. However, ferromagnetic effects due to martensitic transformations in the stainless steel inner form on which the coils are wound have grown with repeated thermal and magnetic cycling. These effect particularly the remanence and the lower harmonic components at the lower dipole field levels.

Model Magnet

The 8° superconducting magnets are of the rectangular aperture "window-frame" type with the iron core surrounding a rectangular cross section dipole coil package. The magnet cross section is shown in Fig. 1. The aperture in the iron is approximately 4-in. high by 6.25-in. wide. The overall dimensions are 14.875-in. high, by 17.125-in. wide. The iron core, closely coupled around the coil, reduces the ampere turns required for magnetic fields below saturation by a factor greater than 2. The images of the coil in the iron give extended dipole sheets, producing very uniform fields below 20kG. Above saturation at the pole surfaces, the ampere turns requirement increases, growing by 21% at 40kG compared to infinite permeability. The systematic aberrations due to saturation require an auxiliary correcting coil which is approximately an aircore sextupole. The excitation required of this correcting coil commences at ~ 20 kG and grows linearly to several percent of the dipole coil ampere turns by 40kG. The combination of the two separate coils, the dipole and the correction, permits precision fields at all levels, as well as providing available sextupole "tuning" where desired.

The dipole coil is wound with 340 turns of a NbTi composite with a rectangular cross section of 0.054-in. by 0.113-in.

The conductor has 1.25 to 1 copper to superconductor ratio and contains 361 filaments of 3 mils diameter, twisted one turn to the inch. Between each single vertical layer of conductor are placed sheets of anodized high purity aluminum. These sheets are

Work performed under the auspices of the U.S. Atomic Energy Commission

grooved to provide vertical LHe channels over 50% of the surface area. The high diffusivity and conductivity of the aluminum provide enhanced thermal and dynamic stability.

TABLE I
20-In. Model Magnet Parameters

Aperture, Diameter	3.375 in.
Magnetic Field Intensity	40kG
Ampere-turns, Dipole Coil	408,000
Ampere-turns, Sextupole Coil	18,000
Current, Dipole Coil	1,200A
Current, Sextupole Coil	300A
Current Density, Dipole Coil Conductor	3.05×10^4 A/cm ²
Current Density, Sextupole Coil Conductor	3.71×10^4 A/cm ²
Stored Energy	48kJ
Inductance, Dipole Coil	55mH

The coil construction techniques and the test assembly of the 20-in. model have been described in more detail.¹ Fig. 2 shows the completed model.

The construction of the 20-in. model was used to develop the techniques used in the construction of the full sized magnets. Indeed these have proceeded with no difficulties in construction. Fig. 3 shows one of the completed 6-ft. long magnets.

Magnet Performance

The 20-in. magnet is extremely stable. It can be simply switched on to or off from its operating field of 37kG. This results in current rise or decay in seconds. The magnet has a solid core, and such treatment results in very large losses. This fact has been confirmed by a wattmeter measurement, as well as by observed pressure fluctuations in the dewar. Nonetheless, the magnet does not go normal. Initial tests were performed with large 120V SCR power supplies with considerable ripple, and the magnet operated up to 40kG. A remote switching failure in one of these supplies resulted in the dipole current supply remaining on after a quench for an extended period. The dewar was boiled dry, which requires energy dissipation 10 times that stored in the magnet. No harm was done to the magnet.

After low voltage, highly filtered power supplies were used, the magnet was excited to above 45kG. No systematic attempt was made to raise this level by repeated quenching.

In Fig. 4 is shown a normalized excitation function for the dipole field of the 20-in. magnet. Computer results assuming Vitrenamel and M-36 permeability data are also shown. Vitrenamel sheet is a low carbon steel which is close in composition to the plate used in the magnet. It suffers some deterioration in permeability compared to thick plate, however, due to the rolling process. In addition, iron at 4°K should have a slightly higher saturation induction than at 300 K. As a result, the fact that the model performs better than computations predict at 27.5kG and 30.6kG

by the equivalent of ~300 gauss is very reasonable. At the highest fields the model saturates more than the computer indicates. This is probably due to the fact that the length of the magnet is only 5 times the vertical gap. The iron core thickness is designed for the infinitely long, two-dimensional flux distribution. The data is taken with a point coil centered in the magnet.

It should be noted that the area enclosed by the up and down sides of the hysteresis loop in Fig. 4 is very small. This results from the fact that the ratio of gap length to iron return length is an order of magnitude greater than in typical low field iron magnets. As a result, even though the iron in the pole surface region is driving very hard into saturation, the sensitivity of such magnets to permeability fluctuations should be comparable to conventional iron magnets excited to their normal saturation levels.

Taking into account the maximum field in the conductor is 10% more than the dipole field, the superconductor peak performance was 80% of short sample current, or 90% of short sample field. However, the official rating on this conductor may be slightly optimistic. Fig. 5 shows the results of some limited tests. The maximum performance of the 20-in. magnet operation is superimposed on the short sample curve. Following study of the full-scale 8^o magnet performance more extensive short sample tests will be made. Finally, a very important point is that at the highest fields no voltage is observed across the magnet. The resistive dissipation in the coil while operating at 40kG D.C. is zero, with an accuracy corresponding to an error of less than 2 watts. This is as expected, since such a coarse strand superconductor should show a very sharp transition from the superconducting to normal state.

Search Coil Measurements

The radial field was measured at 1.513-in. with both short and long coils. The field is expressed as

$B = \sum (A_n r^n \sin(n+1)\theta + B_n r^n \cos(n+1)\theta)$. The sum was carried out to $n = 11$. For no construction or measurement errors, symmetry allows only even n terms in A_n , and no B_n terms. During the latest run, the magnet was repeatedly cycled to 35kG. The raw harmonic analysis results for the short coil during the rise and fall of field are given in Table II. This is at ρ_c , 82% of the radius to superconductor, and is outside the warm bore beam pipe radius (1.438-in.). The amplitudes are normalized to the dipole, $a_n = A_n \rho_c^n / A_0$ and $b_n = B_n \rho_c^n / A_0$. The horizontal reference angle $\theta = 0$ was defined by the phase of $a_{2\theta}$ which is generated at high fields by the correction coil. With the reference angle thus defined, the out of phase dipole was $b_1 = B_1 / A_0 = + (3.3 \pm 1) \times 10^{-4}$ over the complete range of excitation. Therefore, if $\theta = 0$ was redefined by the dipole, the angular offset would only be 3.3×10^{-4} parts, which has a negligible effect on minor components. Also, the jitter in dipole orientation is $\leq 1 \times 10^{-4}$ parts.

Interpretation of Table II is complicated by growing ferromagnetism in the stainless steel inner coil structure of the model. In spite of this, very small errors due to practical construction tolerances are demonstrated. Only the a_n terms are affected; i.e., those with poles at 90° and 270° . The ferrite problem for a will be only briefly summarized, for two reasons: (a) It is eliminated for the 8^o magnets. Each inner structure is one piece (without welds) type 316 stainless steel. (b) It will be seen in the next section that for checking the allowed precision of the model and agreement with computations, the problem can be set aside.

b Terms

None are allowed except by practical errors. The $b_{2\theta}$ term is uniformly 1×10^{-4} . This is the quadrupole of normal orientation; i.e., with a pole at 45° . Similarly, $b_{3\theta}$, $b_{5\theta}$, etc. give the "normal" components where the field is vertical on the horizontal midplane. All are minute. The even n $b_{3\theta}$, $b_{5\theta}$, etc. are the "skew" terms with poles rotated half way

TABLE II

RAW DATA, INCLUDING FERROMAGNETISM IN STAINLESS STEEL
HARMONIC COEFFICIENTS MEASURED DURING A HYSTERESIS LOOP TO 35KG

(n+1)θ	0.53kG		1.2		2.6		5.5		10.9		19.0		32.3kG	
lθ	a _n	b _n												
Rising I	[x10 ⁻⁴]													
3θ/1θ	-334.8	6.8	-198.1	3.7	-114.5	2.2	+20.6	0.6	+2.3	1.2	-7.7	1.1	-6.1	0.7
5θ/1θ	-51.4	0.3	+16.8	1.0	+25.3	0.1	+10.2	0.1	+6.0	0.3	+4.2	0.1	+4.6	0.1
7θ/1θ	+7.6	0.6	+18.7	0.6	+13.4	0.7	+3.1	0.1	+2.9	0.2	+2.2	0.1	+0.8	0.3
9θ/1θ	+10.7	1.4	+1.4	1.0	-2.7	0.1	-7.8	0.5	-5.2	0.0	-4.2	0.0	-21.7	0.0
11θ/1θ	+2.8	0.1	-7.0	0.6	-6.1	0.4	-3.3	0.0	-2.2	0.1	-1.2	0.0	-2.8	0.1
2θ/1θ	+70.2	4.3	+34.5	0.5	+23.8	1.1	+18.1	1.2	+13.5	1.1	+14.1	1.1	+10.8	1.2
4θ/1θ	-10.5	0.3	-5.2	0.2	-4.3	2.1	-2.9	0.0	-2.1	0.2	-2.2	0.2	-1.0	0.7
6θ/1θ	-5.0	1.0	-3.0	1.4	-1.1	0.9	-0.8	0.3	-0.4	0.3	-0.3	0.1	-0.8	0.5
8θ/1θ	+1.4	0.4	+1.0	0.7	-0.7	0.7	+0.4	0.2	-0.1	0.1	+0.1	0.0	+0.8	0.1
10θ/1θ	-1.6	0.2	-0.9	0.1	-0.7	0.5	+0.1	0.1	+0.3	0.3	+0.3	0.3	+0.8	0.7
Falling I														
3θ/1θ	-342.7	7.5	-204.2	3.8	-118.9	2.6	+24.9	1.1	-1.4	0.2	-11.8	1.3	-12.8	0.8
5θ/1θ	-131.5	0.6	-51.7	0.1	-17.1	0.2	-2.6	0.3	+1.9	0.2	+4.5	0.1	+6.0	0.2
7θ/1θ	+3.8	0.9	+12.8	0.9	+9.8	0.1	+3.6	0.2	+2.3	0.2	+2.0	0.1	+0.6	0.3
9θ/1θ	+18.6	2.1	+6.5	0.8	+1.1	0.0	-6.6	0.4	-4.8	0.1	-4.1	0.1	-21.5	0.0
11θ/1θ	+12.8	1.1	+1.2	0.6	-1.2	0.5	-1.9	0.1	-1.2	0.1	-1.2	0.0	-2.9	0.1
2θ/1θ	+73.9	7.1	+39.4	0.7	+24.9	1.0	+17.1	1.0	+14.8	1.1	+15.7	1.1	+10.9	0.9
4θ/1θ	-10.6	3.3	-4.1	0.5	-3.5	0.1	-2.5	0.4	-2.3	0.0	-2.2	0.2	-0.9	0.6
6θ/1θ	-2.9	0.4	-2.6	0.2	-0.9	0.3	-0.9	0.1	-0.4	0.1	-0.6	0.2	-0.6	0.4
8θ/1θ	+1.4	1.3	-1.4	1.4	-1.0	0.9	+0.4	0.4	+0.2	0.2	+0.1	0.1	+0.8	0.3
10θ/1θ	-2.8	1.5	-0.5	0.4	-0.1	0.1	-0.4	0.3	+0.4	0.3	+0.4	0.4	+0.8	0.7
I (amps)	12.9		30.03		63.45		132.5		264.1		460.9		853.0	
Ic (amps)	0		0		0		5.60		5.60		7.22		122.8	

between the poles in the normal orientation. The skew sextupole $b_{23\theta}$, which can be caused by construction errors, is $\lesssim 1 \times 10^{-4}$. In summary, except at very low fields where their absolute magnitude is minute, the lowest order error terms, quadrupole and sextupole are $\lesssim 1 \times 10^{-4}$. All others are a few parts in 10^5 . These errors are small even by conventional magnet standards.

Austenitic 304 Stainless Steel

The austenitic 304 stainless steel rectangular structure, which contributes to the a_n terms, is composed of a welded fabrication of a 0.062-in. tube and stainless steel plate. Welds exist at the top and bottom surfaces at 90° and 270° ; i.e., at the surfaces intersected by a vertical line through the magnet center (Fig. 1). What is to be expected? Martensitic transformations can grow with each temperature cycle and are affected by applied strain. Two products occur, one of which is ferromagnetic.² Ferrite content can vary widely. Maximum permeability occurs at low fields, but flux saturation typically requires $\sim 10\text{kOe}$. Weld material can be quite ferromagnetic with strong local perturbations.

To the extent the ferrite is statistically uniform over the structure, it contributes only to the allowed terms, with lower order multipoles surely predominant. This is consistent with observations of its remanent and dynamic effect: $a_{45\theta}$ is $\sim 10\%$ of $a_{23\theta}$, and higher terms are negligible. If the welds at 90° and 270° are magnetically non-uniform, this will concentrate flux at either the top or bottom poles. Such asymmetry will produce the skew term $a_{12\theta}$, $a_{34\theta}$, etc., with poles located at 90° and 270° . This again does occur, with $a_3 \sim 20\%$ of a_1 .

In summary, over an extended period with several magnet cooldowns and repeated excitation runs, the magnitude of ferromagnetism in the stainless steel continues to grow. This contributes only to the a_n terms. The b_n terms, which would only be effectedⁿ by higher order asymmetry in the stainless show no ferrite contribution.

The a_n Terms with n Odd

The skew quadrupole $a_{12\theta}$ has become quite large with a very small hysteresis loop width. The amplitudes are almost equal for rise and fall all the way down to remanence (not shown in Table II). This skew term is not due to asymmetrical diamagnetism in the superconductor, which would produce a large loop width at low fields (see $a_{45\theta}$ later). Both $a_{12\theta}$ and (very small) $a_{34\theta}$ have grown in step both in remanence and dynamic amplitudes since the first experiments and with the same characteristic B dependence. Any skew quadrupole $a_{12\theta}$ due to construction errors would be a constant like b_1 . The upper limit on a_1 , apart from the stainless effect, is small compared to 10×10^{-4} . Finally, the integral coil results, which sample all the ferrite, have consistently shown an a_1 of $\sim 50\%$ of the point coil data and of opposite sign.

The a_n Terms with n Even

The only terms allowed by symmetry. The 20-in. model is not an optimum "paper" design; as computed $a_{23\theta} = -12.9 \times 10^{-4}$ for μ large and the correction current $I_c = 0$. Remanence and hysteresis in the iron and superconductor will contribute, as well as the stainless steel. The small loop width of $a_{23\theta}$ indicates that superconducting diamagnetism is a relatively small contributor. A low field a_2 hysteresis tail (partly shown in Table II) is similar to that of the dipole 1θ (Fig. 4). This tail is also characteristic of conventional ferromagnets. The remanent sextupole field $A_{23\theta}^2$ at the time of Table II was -10G .

This is double that of any earlier run, and contains normal iron remanence plus the ferrite. The hysteretic tail is over by 2.6kG, blending smoothly from remanence into a -22G offset compared to predictions. The a_2 offset due to stainless, grows slowly with B, saturates and diminishes with the same functional relationship as a_1 and a_3 . The offset pattern like remanence, has grown in magnitude.

The $a_{45\theta}$ data, with rise and fall averaged because of large diamagnetism, show the same synamic ferrite pattern, but much smaller ($\sim 3\text{G}$ overall) and reversed in sign. Both have the same remanent sign with the ferrite opposing the overall remanent, a_4 . This is consistent with the fact that of all the remanent terms, only a_4 has decreased as the ferrite grows. Understanding aside, the data above 5kG in Table II is of most interest. The large $a_{23\theta}$ at 5.5kG is due to missettings of I_c . The $a_{23\theta}$ average at 32.3kG, where ferrite should make the smallest contribution, was compared with computer predictions. The magnet permeability was extrapolated from the dipole comparisons at $\sim 31\text{kG}$ in Fig. 4. The computer agrees to 1×10^{-4} . The ferrite effect is several times larger than this, so the result is fortuitous. Nevertheless, a_2 is correctly predicted to considerably better than 1×10^{-3} .

Apart from $a_{45\theta}$ diamagnetism, $a_{45\theta}$, $a_{67\theta}$, etc. are well behaved and agree with predictions. The large $a_{89\theta}$ at 32.3kG is generated by the correction coil when I_c is large. For the present magnet circuit, superconducting diamagnetism is almost entirely due to the auxiliary correction coil.³ This produces predominantly $a_{45\theta}$. During the rise this effect contributes $a_4 = +6.4 \times 10^{-4}$ at 5.5kG. This should diminish as B^{-2} .

Allowed a_n With $a_{23\theta}$ Tuned To Zero

It is evident that practical error terms are very small in the 20-in. model, apart from the ferrite in the stainless steel. The remaining questions are (a) how well does the data confirm the computer predictions, and (b) how good is the magnet? Extensive experimental and computed data exists on the effects of incremental changes δI_c in the correction coil current. This permits adjustment of $a_{23\theta}$ to zero or other standard value. Such small adjustments have almost vanishing effect on higher allowed terms; i.e., δI_c produces essentially pure $a_{23\theta}$ change. For example, tuning the 5.5kG data of Table II to zero by adding $a_{23\theta} = -22.8 \times 10^{-4}$ changes $a_{89\theta}$ by $+1 \times 10^{-4}$. All other terms change by considerably less. At 10.9, 19.0, and 32.3kG, tuning $a_{23\theta}$ to zero changes all higher terms negligibly ($\ll 1 \times 10^{-4}$). Note this procedure makes no assumptions about subtracting a background $a_{23\theta}$ due to ferrite, but simply corrects for it. The ~ 10 times smaller $a_{45\theta}$ ferrite contribution, however, does give a residual error at the $\sim 1 \times 10^{-4}$ level for comparing computer and experiment at the fields of interest. This could have been subtracted

TABLE III

HARMONIC COEFFICIENTS OF 20-IN. MAGNET ALLOWED BY SYMMETRY WITH SEXTUPOLE TUNED TO ZERO						
B_0 (kG)	5.5		19.1		38.3	
$\frac{\rho}{\rho_{\text{max}}}$ (%)	82	50	82	50	82	50
$3\theta/1\theta$	0.	0.	0.	0.	0.	0.
$5\theta/1\theta$	+3.4	+0.50	+3.3	+0.49	+7.0	+1.03
$7\theta/1\theta$	+4.2	+0.24	+2.1	+0.12	+2.3	+0.13
$9\theta/1\theta$	-5.4	-0.12	-4.2	-0.09	-30.6	-0.66
$11\theta/1\theta$	-2.2	-0.02	-1.2	-0.01	-3.3	-0.03

The coefficients are expressed in units of 1×10^{-4} .

out. It was not because of the wish that Table III show show the magnet as it is. At 19kG with the sextupole tuned out, all measured allowed multipoles agree with co computations with $<1 \times 10^{-4}$ error.

Table III gives the tuned data at 5.5 and 19.kkG. The 38.3kG data is from a separate, higher field run. The so-called harmonic coefficients measured at radius ρ in Tables II and III are actually the amplitudes of the multipoles normalized to the dipole; i.e.,

$$\frac{A_n \rho_c^n}{A_0}$$

and thus dimensionless. The amplitudes at a radius of 50% to superconductor, $\rho_0 = \frac{1}{2} \rho_{max}$, are also shown. If $\rho_{max} = 2$ (for example, 2 inches), then $\rho_0^n = 1^n = 1$, and the 50% columns are true coefficients with dimensions ρ_0^{-n} (in. $^{-n}$ in our example).

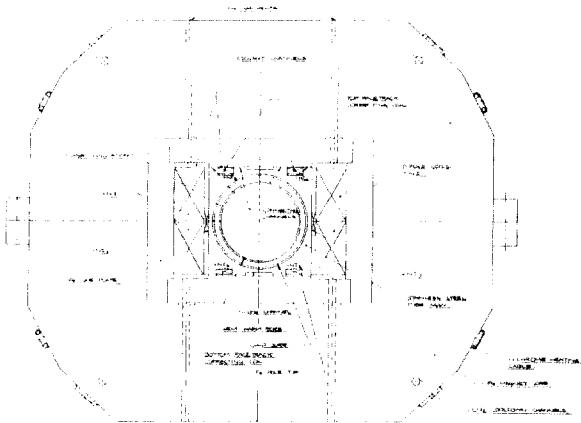


Fig. 1 - Cross-section of the 8° Superconducting Magnet

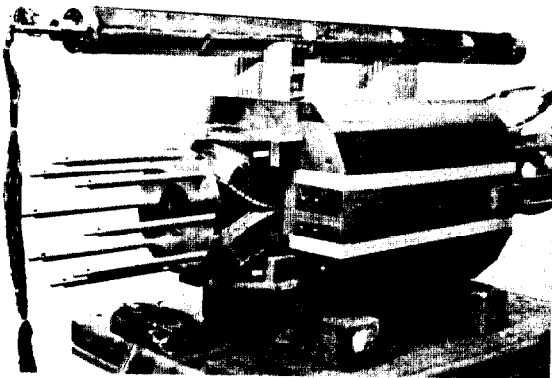


Fig. 2 - Completed Assembly of 20-in. Magnet with Harmonic Search Coil



Fig. 3 - 8° Superconducting Magnet Module Prior to Installation in Dewar

Field Uniformity of Allowed Terms, Sextupole Tuned Out

The field uniformity $\Delta B/B$ on the horizontal and vertical midplanes is shown at 19.kkG in Fig. 6 as a function of radius. The difference between experiment and predictions is also shown. The field is everywhere flat to $\sim 1 \times 10^{-4}$. The first derivative B'/B (in. $^{-1}$) is $<3 \times 10^{-4}$ to 70% radius. The second derivative B''/B (in. $^{-2}$) is $<1 \times 10^{-3}$ to beyond 60% radius (Fig. 7). The 5.5kG data is almost identical, being a few percent worse. This field quality is much better than required for its application, although better designs now exist. Fig. 8 shows $\Delta B/B$ at 38.3kG. This is $\leq 1 \times 10^{-4}$ to $\sim 55\%$ radius. B'/B is $<3 \times 10^{-4}$ to $\sim 57\%$ radius. B''/B (Fig. 9). $\leq 1 \times 10^{-3}$ to almost 50%. The deviation at 38kG is due to large $a_{9\theta}$, which in later designs has been greatly reduced. Note that the units are for a 4-in. diameter magnet. For the 20-in. magnet, B'/B is increased by 1.06 for in. $^{-1}$, and B''/B by 1.12 to be in units of in. $^{-2}$ in Figs. 7 and 9.

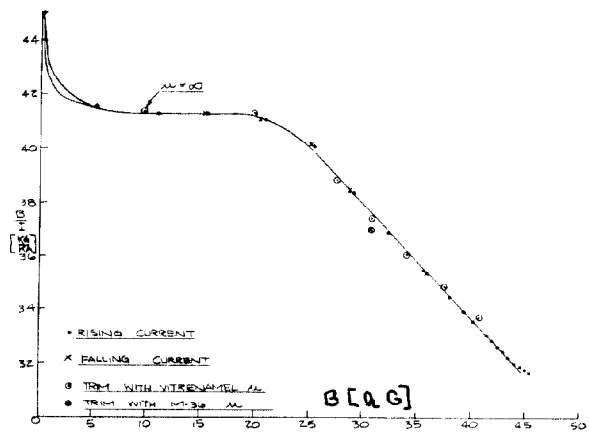


Fig. 4 - Normalized Excitation Function for 20-in. Magnet

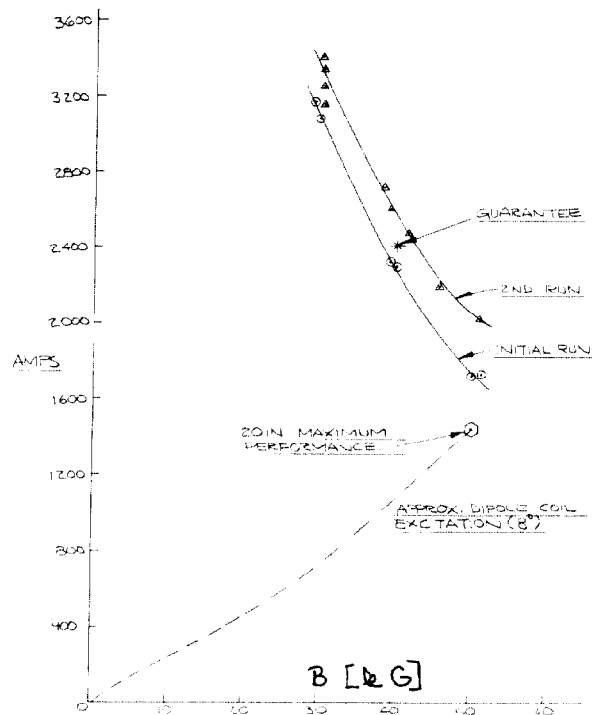


Fig. 5 - Short Sample Superconductor Tests

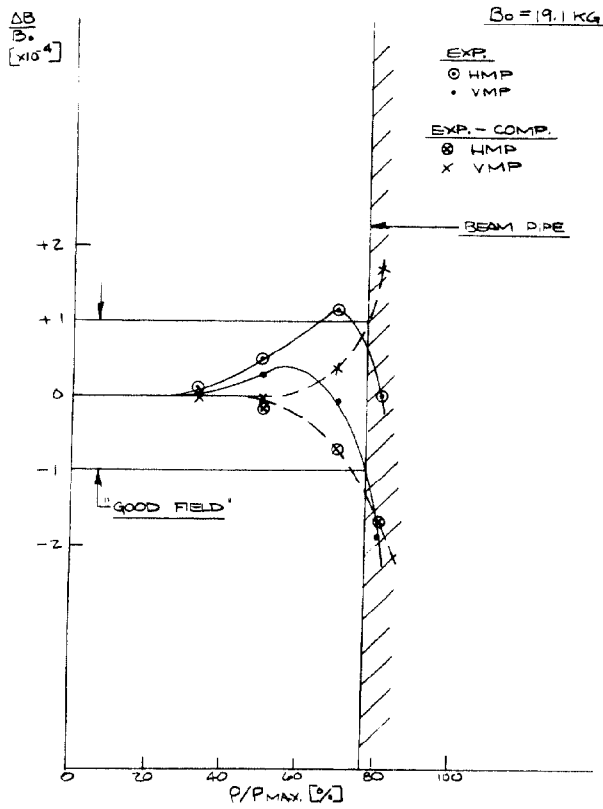


Figure 6.

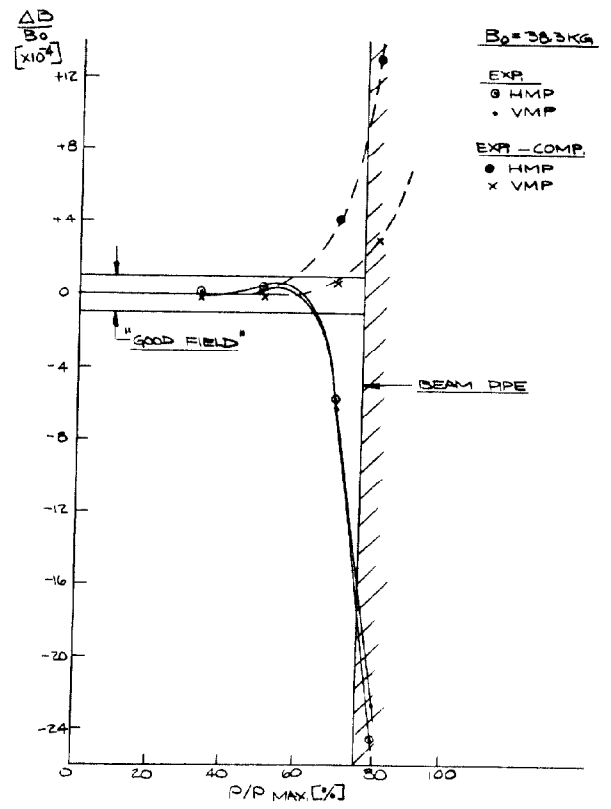


Figure 8.

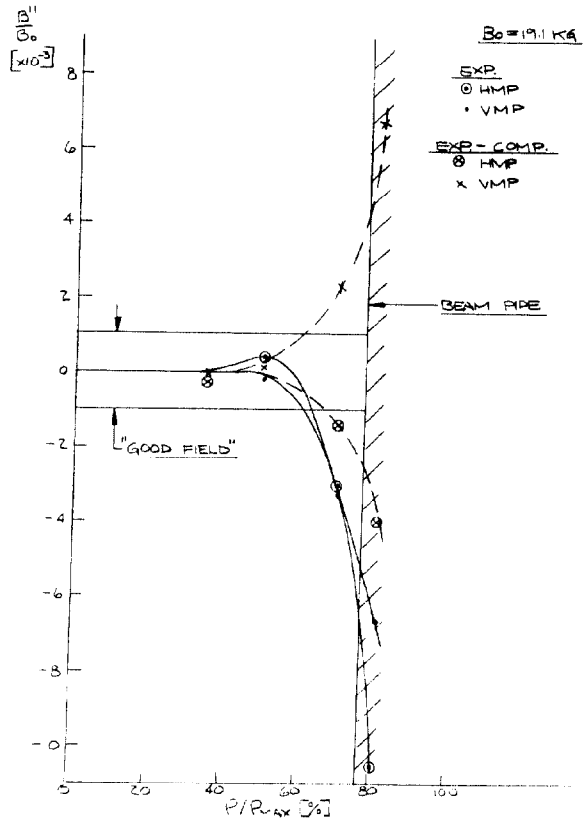


Figure 7.

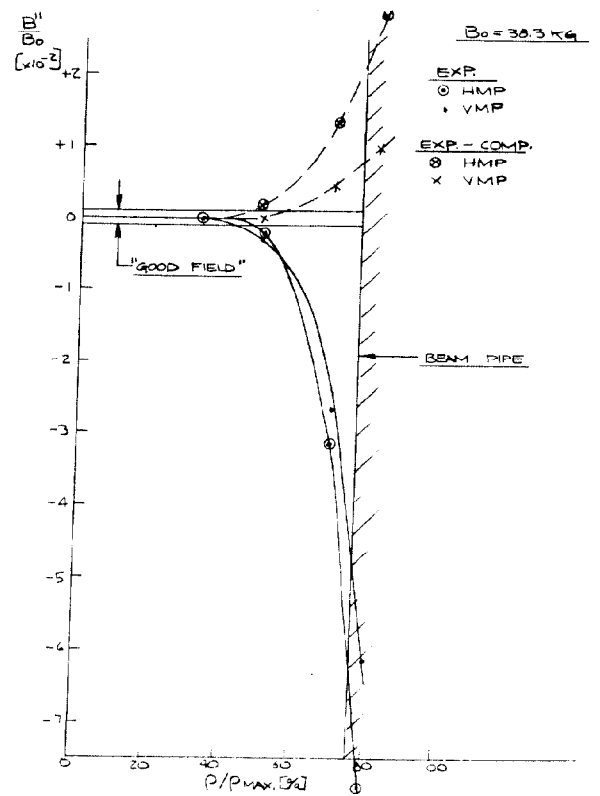


Figure 9.

References

1. J. Allinger et al., in Proceedings of The Fourth International Conference on Magnet Technology (CONF-720908) p. 758(1972).
2. R.P. Reed and C.J. Guntner, Trans. of the Metallurgical Society of AIME, Vol. 230, p.1713(1964).
3. G. Danby, et al., in Proc. of The Fourth International Conference on Magnet Technology (CONF-720908) p.334 (1972).